A Numerical Study of the Effect of GOES Sounder Cloud-Cleared Brightness Temperatures on the Prediction of Hurricane Felix

Xiaolei Zou[1], Qingnong Xiao[1],
Alan E. Lipton[2], and George D. Modica[2]

1. Department of Meteorology, Florida State University, Tallahassee, Florida
2. Atmospheric and Environmental Research, Inc., Cambridge, Massachusetts

1

19991122 061

Abstract

The influence of satellite brightness temperature data on the retrospective numerical prediction of Hurricane Felix is investigated. Satellite data are included as an augmentation to bogus data assimilation (BDA) procedure using a mesoscale adjoint modeling system. Assimilation of satellite brightness temperature data was found to have positive impact on both the intensification and track forecast of the hurricane. The improvements made by the simulations using satellite brightness temperatures were realized by intensifying low-level warm ridge located west of the hurricane, reducing the amount of water vapor below 500 hPa over most areas where satellite data are available, and modifying the structures of the initial vortex in the model initial condition. Although being located over a region devoid of satellite data, the initial vortex obtained using both the satellite and bogus surface low data is more realistic than the one using only the bogus data. Despite the fact that the forecast (3.5 days) using only the bogus surface low at the initial time was quite good, track and intensity forecasts beyond 2 days of model integration were shown to be further improved by including satellite data in the initialization procedure. Differences in the prediction of Hurricane Felix with and without satellite data were also found in the prediction of upper-level jet, the cold temperature trough ahead of the hurricane, the size of the hurricane eye, and the location of maximum rainfall during the 3.5 day forecast period. While the focus of this study is to assess the impact of the direct use of satellite brightness temperature data on hurricane prediction, we also noted that the BDA experiment assimilating only the bogus data shows a positive impact of the BDA generated hurricane on the environmental flow, as verified by satellite observations.

1

1 Introduction

Since the early 1960s, meteorological, hydrological and oceanographic data from satellites have had a major impact on environmental data analysis, weather forecasting, and atmospheric research in the United States and throughout the world (Menzel and Purdom 1994). While initially designed for producing images of the earth's cloud cover, the satellite instrumentation has been constantly improved to provide quantitative information about the atmosphere. There has been a realization of the potential that such quantitative observations, received from either polar-orbiting or geostationary satellite ranging from visible, infrared to microwave frequencies, would have in the applications of synoptic weather analysis and numerical weather prediction.

Improvement of the large-scale analysis over data-sparse regions using TOVS radiance data is reflected in an increased global forecast skill of operational numerical weather prediction in the Southern Hemisphere (Andersson et al. 1992; Eyre et al. 1993; Derber and Wu 1998). Satellite observations, which are available at a resolution of about 30 km or higher, are important for hurricane modeling since the routine rawinsonde and ship data are too sparse to capture many important mesoscale features in the initial condition for hurricane simulation. It will become an even more serious problem with the rapid increase of model resolution for hurricane simulation. Several studies investigated the impact of satellite-retrieval products (such as rain rate) on the hurricane initialization and prediction (Krishnamurti et al. 1995; Peng and Chang 1996; Karyampudi et al. 1998; Xiao et al. 1999). Satellite observations in these studies were incorporated into the forecast model through some kinds of reverse cumulus parameterization procedures. Impact of the direct use of satellite brightness temperatures, instead of their retrieved products, needs to be assessed.

The work summarized in this paper presents part of the effort funded by the Air Force OSR to assess the impact of GOES-8 satellite brightness temperature data on hurricane prediction. The case chosen for this study is Hurricane Felix from the 1995 Atlantic hurricane season, which lasted from 12 August to 21 August 1995. Figure 1 shows the GOES-8 infrared cloud image at 2346 UTC 15 August (Fig. 1a), and the data distributions of the GOES-8 observed brightness temperatures at 00 UTC 16 August 1995 (Fig. 1b). Due to the data void

2

region over the hurricane (see Fig. 1b), a vortex bogus initialization is needed for a successful hurricane simulation and then to properly assess the impact of the GOES-8 satellite data. In order to allow a direct use of satellite observations in such a hurricane initialization, we developed a variational bogus data (BDA) scheme in which a surface low is bogused into a 4-dimensional variational data assimilation procedure. The technical details and the numerical performance of the BDA hurricane initialization procedure can be found in a paper by Zou and Xiao (1999). It was shown that a model initial condition, describing consistently the dynamic and thermodynamic structure of a hurricane vortex, can be generated by fitting the forecast model to a bogus surface low specified based on a few observed and estimated parameters. As a result of BDA, dramatic improvements occurred in the prediction of the track, intensity and structure of Hurricane Felix. The present paper demonstrates the feasibility of including satellite brightness temperature observations directly into the BDA procedure and assesses the impact of environmental satellite data on the hurricane initialization and prediction. We first developed the techniques necessary to incorporate the satellite data into a hurricane prediction model. This requires the development of the adjoint of a radiative transfer model and the proper linkage of both the radiative transfer model and its adjoint into the MM5 adjoint model system (Zou et al., 1995; Zou et al., 1997). We then assessed the impact of satellite data available in the surroundings of the hurricane for the prediction of hurricane track and intensity change during the period from 12 UTC 15 to 00 UTC 19 August 1995, during which Felix made a north-eastward recurvature from its north-westward track.

The paper is arranged as follows. In section 2, we provide a brief description of GOES-8 brightness temperature measurements, the observation operator, the quality control, and the measurement errors. Section 3 reports the sensitivities of brightness temperatures at different channels to several assigned temperature and humidity profiles. The data assimilation procedure, forecast model, and experiment design are presented in section 4. The model initial conditions, obtained by BDA scheme with and without the GOES-8 brightness temperatures, are described and compared in section 5. Impact of the bogus surface pressure and GOES-8 cloud-cleared brightness temperatures on the prediction of hurricane Felix is presented in section 6. The paper concludes in section 7.

3

2 GOES-8 satellite data and a radiative transfer model

2.1 A brief description of GOES-8 satellite data

The new series of Geostationary Operational Environmental Satellites (GOES) beginning with GOES-8 was launched on 13 April 1994. It has been designed with separate imaging and sounding instruments to support the requirements of the modernized National Weather Service in the 1990s. It is three-axis stabilized to improve instrument performance and enable more efficient data gathering by both the imager and sounder. The GOES-8 sounder includes 18 thermal infrared bands plus a low-resolution visible band. The spectral bands are sensitive to temperature, moisture, and ozone. Significant improvements in data quality and information content, with respect to previous geostationary satellites, encourage the use of these data in many areas of research (Smith and Lee 1995).

The potential use of satellite data to significantly contribute to hurricane forecasting, where models are initialized mostly over oceanic regions, needs to be fully assessed. However, the "optimal" use of satellite data faces many challenges. Among these are (i) the quality control of the observed brightness temperatures to remove possibly cloud-contaminated or erroneous data, and (ii) the direct use of brightness temperature data instead of the retrieval products. The later requires a computationally efficient radiative transfer model which computes the brightness temperatures from the meteorological variables. One such model for the use of GOES-8 brightness temperatures, a radiative transfer model, is illustrated in the following section.

2.2 Radiative transfer model

The satellite brightness temperatures can be computed from the atmospheric profile through a so-called radiative transfer model written symbolically as:

$$\mathbf{y} = \mathbf{H}(\mathbf{x}) \tag{1}$$

where $\mathbf{H}$ is an observation operator calculating the brightness temperatures based on model state, $\mathbf{x}$ represents the input vector of model state variables to the radiative transfer model, and $\mathbf{y}$ is the vector of the simulated brightness temperatures at various channels. In

4

general, the vector **x** includes the vertical profiles of temperature and humidity, surface skin temperatures, and surface pressure.

Table 1: Radiative-transfer-model layers (fixed pressure levels in hPa)

0.1	0.2	0.5	1.0	1.5	2.0	3.0	4.0	5.0	7.0
10.0	15.0	20.0	25.0	30.0	50.0	60.0	70.0	85.0	100.0
115.0	135.0	150.0	200.0	250.0	300.0	350.0	400.0	430.0	475.0
500.0	570.0	620.0	670.0	700.0	780.0	850.0	920.0	950.0	1000.0

In this research, we adopted a radiative transfer model similar to that of Eyre and Wolf (1988) and Eyre (1991), with some modifications made to fit the GOES-8 sensor observation. The input variables of our radiative transfer model, the vector **x**, are temperature and humidity profiles, surface pressure, and surface skin temperature. The forward model consists of 40 layers ranging from 0.1 hPa to 1000 hPa (Table 1). Humidity is expressed as the logarithm of specific humidity, since forecast errors in this quantity are more constant than in specific humidity itself. Because the radiative-transfer-model layers are not necessarily consistent with the model layers on which values of temperature and humidity are available, interpolation or extrapolation is needed. In this study, a linear interpolation (extrapolation) scheme in $log(p)$ is adopted to generate temperature and humidity at the 40 radiative-transfer-model layers from the 27 σ-layer model analysis and/or forecast. The input humidity profile required by the radiative transfer model is limited to the lowest 15 levels (i.e. up to 300 hPa). It is then extrapolated to give a reasonable stratospheric profile as follows:

$$q_n = \begin{cases} max\{q_{300}(\frac{p_n}{300})^3, q_{min}\}, & \text{if } 300 > p_n \geq 70 \ hPa; \\ q_{min}. & \text{if } p_n < 70 \ hPa, \end{cases} \tag{2}$$

where $q_{min} = 0.003$ g kg-1, p_n and q_n are pressure and specific humidity at the nth layer.

The radiative transfer model consists of an algorithm for the calculation of the transmittance (τ_α) profile for the αth channel, which starts from the top of the atmosphere (where $p_0 = 0$, $\tau_{\alpha,0} = 0$):

$$\tau_{\alpha,n} = \tau_{\alpha,n-1} exp(Z), \tag{3}$$

where

$$Z = sec\Theta \sum_{m=1}^{10} a_{mn}^{\alpha} X_{mn} + (sec\Theta - 1) \sum_{m=1}^{4} b_{mn}^{\alpha} Y_{mn}, \tag{4}$$

where n denotes vertical layers of the radiative transfer model, Θ the satellite zenith angle and X_{mn} and Y_{mn} are quantities depending on the estimated atmospheric state (see Eyre and Wolf 1988):

$$X_{1n} = \delta T_n, \quad X_{2n} = \delta T_n^2, \quad X_{3n} = \sum_{k=1}^{n} \delta T \triangle p_k / p_n,$$

$$X_{4n} = 2 \sum_{k=1}^{n} \delta T_k p_k \triangle p_k / p_n^2, \quad X_{5n} = \delta q_n, \quad X_{6n} = \delta q_n^2,$$

$$X_{7n} = \sum_{k=1}^{n} \delta q \triangle p_k / p_n, \quad X_{8n} = 2 \sum_{k=1}^{n} \delta q_k p_k \triangle p_k / p_n^2,$$

$$X_{9n} = \delta q_n \delta T_n, \quad X_{10n} = 1,$$

$$Y_{1n} = 1., \quad Y_{2n} = X_{4n}, \quad Y_{3n} = X_{6n}, \quad Y_{4n} = sec\Theta - 1$$

where $\triangle p_k = p_k - p_{k-1}$ (with $p_0 = 0$), and T_k and q_k are the mean temperature and specific humidity in layer $\triangle p_k$. We found that the following two formulae to calculate δT_k and δq_k with two layers gives significantly lower errors than if the values just for the k-th level are used.

$$\delta T_k = \frac{(T_k - \overline{T}_k + T_{k-1} - \overline{T}_{k-1})}{2} \tag{5}$$

$$\delta q_k = \frac{(q_k - \overline{q}_k + q_{k-1} - \overline{q}_{k-1})}{2} \tag{6}$$

In (2.5) and (2.6) $\overline{T}_k$ and $\overline{q}_k$ refer to the reference quantities.

In order to compute transmittance, the zenith angle Θ must be known. For GOES-8, every individual field of view (IFOV) has a unique zenith angle. The coefficients a_{mn}^{α} and b_{mn}^{α} are found by multiple regression which fits to the line-by-line radiative transfer model (LBLRTM) (see Clough et al. 1992) and are supplied as input constant quantities to our radiative transfer model.

The transmittances calculated above are used to compute radiance (R_{α}) within the integration of radiative transfer equation (Liou 1980). For infrared channels, the clear-column radiance of channel α is given by:

$$R_{\alpha} = R_{\alpha}^{s} + R_{\alpha}^{u} + R_{\alpha}^{d}, \tag{7}$$

6

where R_α^s is the contribution from the surface, R_α^u is the contribution from atmospheric direct upward emission, and R_α^d is the contribution from atmospheric downward emission reflected back from the surface, which was neglected from this study.

The surface contribution is given by:

$$R_\alpha^s = \varepsilon_\alpha B_\alpha(T_s)\tau_\alpha(p_s),\qquad(8)$$

where ε_α denotes surface emissivity at frequency α, B_α is the Planck function, T_s is surface temperature, p_s is surface pressure and $\tau_\alpha(p_s)$ is the transmittance from the Earth's surface to space. Over land, the surface emissivity ε_α was assumed to be 0.97 for channels 1-12 and 0.96 for channels 13-18. Over ocean, the surface emissivity was 0.98 for all channels.

The contribution of direct atmospheric upward emission, R_α^u, is obtained as a sum of the contributions from all emitting layers:

$$R_\alpha^u = \frac{1}{2}\sum_{k=1}^{N} \left[B_\alpha(T_k) + B_\alpha(T_{k-1})\right]\left[\tau_{\alpha,k-1} - \tau_{\alpha,k}\right],\qquad(9)$$

where T_k is the temperature at atmospheric level k and $\tau_{\alpha,k}$ is the transmittance in channel α from level k to space.

The brightness temperature is converted from radiance using the inverse Planck function.

2.3   Data quality control and error statistics

Infrared satellite data were collected from the sounder aboard GOES-8 satellite at the Air Force Research Laboratory (AFRL) using the AFRL Interactive Meteorological System (AIMS) facility. The GOES-8 sounder data were cloud-cleared to correct for the complicating effects that hydrometeors have on the interpretation of infrared brightness temperatures. Cloudy GOES-8 individual fields of view (IFOVs) were identified using a person-computer interactive cloud-clear discrimination program that operated on images made with data from the visible channel and from the infrared channels at 3.7 and 11.0 micrometers. To create a single sounding field of view (SFOV), a set of IFOVs were averaged horizontally. The purpose of the averaging is to compensate for data noise. We used the method outlined in Lipton (1998) to select a set of averaging areas that would minimize the gaps in coverage caused by clouds. Data were averaged from 3x3 boxes of GOES-8 IFOVs, resulting in SFOVs

of approximately 30 × 30 km². At least four clear IFOVs were required to make a SFOV, and an isolation limit of 9 clear IFOVs was used.

Following the cloud and precipitation clearing steps outlined above, the satellite data were further processed by removing the bias between the satellite brightness temperatures and those calculated from co-located radiosonde observations. For this we used a shrinkage estimator (Fleming et al. 1991) which is a modified regression technique. In our application of the shrinkage estimation technique, we used as predictors the satellite sounder channels, the latitude, and the satellite zenith angle of the satellite observations. Table 2 gives the GOES-8 instrument noise errors (E_{ins}) and the forward model errors (E_{fwd}). Values of E_{ins} were computed using a statistical data analysis method (Hillger and Vonder Haar 1988). The forward model errors E_{fwd} were evaluated from comparison between the "fast" forward model and the slow LBLRTM. The error variances of GOES-8 radiance for each channel are then calculated by

$$Var = E_{fwd}^2 + \frac{E_{ins}^2}{n} \tag{10}$$

where n is the number of samples averaged for the given IFOV. The error variance of brightness temperature is computed by multiplying the radiance error variance by $(dT_b/dR)^2$, which is the derivative of the brightness temperature with respect to radiance based on the Planck function.

3 Sensitivity analysis of brightness temperatures with respect to T and q profiles

GOES-8 sounders measure brightness temperatures from 18 infrared spectral bands that are sensitive to the atmospheric temperature and moisture at various heights. In order to assess the sensitivity of the brightness temperatures with respect to perturbations in different atmospheric state, adjoint sensitivity analysis was performed. A simple response function was defined as

$$J_\alpha = J_\alpha(T, q, T_{sk}, p_s) = T_b(\alpha) \tag{11}$$

Table 2: Table of errors for the GOES-8 satellite radiance

Channel	wavenumber (cm^{-1})	wavelength (μm)	E_{ins} $(mW(m^2\ sr\ cm)^{-1})$	E_{fwd} $(mW(m^2\ sr\ cm)^{-1})$
1	680.71	14.71	1.030	0.036
2	695.73	14.37	0.790	0.028
3	711.88	14.06	0.720	0.124
4	732.50	13.96	0.640	0.159
5	747.53	13.37	0.560	0.183
6	790.40	12.66	0.340	0.250
7	829.07	12.02	0.320	0.228
8	906.55	11.03	0.250	0.188
9	1029.55	9.71	0.190	0.539
10	1339.55	7.43	0.130	0.111
11	1422.01	7.02	0.073	0.110
12	1535.43	6.51	0.104	0.054
13	2184.93	4.57	0.013	0.022
14	2207.49	4.52	0.008	0.012
15	2247.11	4.45	0.009	0.003
16	2421.74	4.13	0.005	0.036
17	2509.51	3.98	0.007	0.012
18	2666.41	3.74	0.006	0.001

where $T_b(\alpha)$ is the brightness temperature at the α channel, T the temperature, q the specific humidity, T_{sk} the surface skin temperature, and p_s the surface pressure. In our study, T_{sk} is fixed and all the others (T, q, and p_s) are taken as input variables to the radiative transfer model and will be represented by the vector $\mathbf{x}$.

The sensitivity of J_α with respect to $\mathbf{x}$, expressed as VJ, is usually defined as

$$VJ_\alpha(\mathbf{x}, \Delta\mathbf{x}) = (\nabla J_\alpha)^T \Delta\mathbf{x} \equiv (\hat{\mathbf{x}})^T \Delta\mathbf{x} \qquad (12)$$

where $\hat{\mathbf{x}}$ is the result of the adjoint model integration with a unit input for the adjoint variable of the brightness temperature at channel α and zero value for the adjoint brightness temperature variables at other channels.

If a variation occurs solely in the lth component of the control variables $\mathbf{x}$, we denote by $\Delta \mathbf{x}^l$ the corresponding vector of variation:

$$\Delta \mathbf{x}^l = (0, \cdots, \Delta x^l, \cdots, 0)^T \tag{13}$$

and denote the corresponding sensitivity by VJ_α^l. The relative sensitivity S_l is defined as the non-dimensional quantity (Zou et al. 1993):

$$S_l = \frac{VJ_\alpha^l}{J_\alpha} \left(\frac{\Delta x^l}{x^l} \right)^{-1}. \tag{14}$$

The magnitude of the relative sensitivity serves as a guide to ranking the importance of different components in the input variables $\mathbf{x}$. A plot of the vertical profile of the relative sensitivity, for example, will indicate where the most sensitive ranges of height are for brightness temperature information available at a certain channel.

Figure 2 shows the distribution of the sea-level pressure (SLP) at 12 UTC 15 August 1995 from the NCEP analysis enhanced by MM5 (the Penn State/NCAR nonhydrostatic mesoscale model version 5) data pre-processing procedure. At this time, Hurricane Felix (1995) was located off the east coast of the United States over the ocean. We randomly selected 8 points inside and outside the hurricane ("star" in figure 2 denotes the points that are selected). The relative sensitivities of the brightness temperatures with respect to temperature and humidity profiles at these 8 points were calculated and the numerical results are shown for example in Fig. 3 for channels 6 (12.66 μm, top panels) and 11 (7.02 μm, bottom panels), respectively. We note that the sensitivity profiles for the same channel show, in general, similar variations with height for all the points selected, although these 8 points represent different atmospheric profiles. This is true for other channels (figures omitted). The thick dashed line in figures 3 and 4 are the mean profile of the relative sensitivities averaged over the eight points.

Knowing that the vertical distribution of the relative sensitivities of the brightness temperature at a selected channel with respect to temperature (or specific humidity) does

not vary much from one sounding to the next, what are the differences of the relative sensitivities of the brightness temperature at various channels? Figure 4 shows the the relative sensitivities of the brightness temperatures at various channels, averaged over the 8 selected soundings. An important feature is that sensitivities of brightness temperatures to temperature are positive at all channels (Fig. 4). The higher the temperature, the larger the brightness temperature. The sensitivity to temperature is not uniform at different levels and the level at which the brightness temperature is most sensitive varies with channels. The peak levels of relative sensitivity for channels 1, (14.71 μm), 2 (14.37 μm), 11 (7.02 μm), and 12 (6.51 μm), are above or around 200 hPa. For channels 3 (14.06 μm), 4 and 10 (7.43 μm), the largest sensitivities occur at mid troposphere. The brightness temperatures at channels 5-8, 13-14, 16-18 are most sensitive to temperatures in the low troposphere. Most mid-wave band channels (channel 13-18 with 4.57 μm to 3.74 μm) show the largest sensitivity of the brightness temperatures to the temperature at low levels except channel 15. Sensitivities of brightness temperatures with respect to moisture profile are negative at all channels (figure 4). In other words, the more moist the atmosphere, the lower is the GOES-8 satellite detected brightness temperature. The level of the largest sensitivities of the brightness temperatures are in the low troposphere at channels 5-9, 13-14, 16-18 and the upper troposphere at channels 10-12. Very small water vapor sensitivities are observed for channels 1-4 and 15.

These sensitivity analyses imply that observational information in the GOES-8 brightness temperatures is likely to have impact on the atmospheric thermodynamic state in all levels.

4 Incorporating GOES-8 brightness temperatures into the BDA hurricane initialization scheme

4.1 Cost function formulation and the two BDA experiments

There were 12 time levels when observations of GOES-8 brightness temperature observations were available in the 6-h window from 12 UTC to 18 UTC 15 August 1995. Specifically, the GOES-8 observations took place at $t = 0, 46, 88, 107, 148, 167, 208, 226, 268, 287, 328$, and

346 minutes after 12 UTC August 15, 1995. Figure 5 plots the locations of all the brightness temperature observations that were available over the assimilation domain during the 6-h time window, and that were incorporated into the BDA procedure. Satellite data were available over most areas except the initial vortex region and the southeast corner of the model domain B on which the data assimilation experiments were carried out. To assess the impact of these satellite data on the 2-3 day prediction of the hurricane, an initial bogus vortex was needed to compensate for the satellite data void over the initial vortex region. We thus developed, as the first step, a variational bogus data assimilation (BDA) scheme which makes use of a bogus surface low. The BDA scheme and its numerical performance on the initialization of a mature hurricane and the subsequent prediction were presented in Zou and Xiao (1999). In the study reported here, we included the satellite data into the BDA procedure, which included a bogus SLP field as shown in Fig. 5. The bogus surface low was specified using the Fujita formula with the observed central value of SLP and the radius of maximum low-level wind as the input to the axisymmetric vortex (see Zou and Xiao 1999 for details).

The hurricane initialization was carried out by minimizing a cost function which measures the discrepancy between the model predicted and specified sea-level pressures representing the bogus surface low , J_{bg}, and a cost function including also the distance between model predicted and GOES-8 observed brightness temperatures, J_{bgsat}. A simple background term J_b is always included in the cost function. Mathematically, they can be expressed as:

$$J_{bg}(\mathbf{x}_0) = \sum_{t_m} \sum_{i,j \in \mathcal{R}} (P - P^{bogus})^T W_P (P - P^{bogus}) + J_b, \qquad (15)$$

and

$$J_{bgsat}(\mathbf{x}_0) = \sum_{t_n} \sum_{\vec{r}_k} (T_b - T_b^{GOES-8})^T W_{bt} (T_b - T_b^{GOES-8}) + J_{bg}, \qquad (16)$$

where

$$J_b(\mathbf{x}_0) = \frac{1}{2} \{\mathbf{x}_0 - \mathbf{x}_b\}^T W_b \{\mathbf{x}_0 - \mathbf{x}_b\}. \qquad (17)$$

Here, the summation over t_m in (15) was carried out over a half-hour window at 5 minute intervals starting from t_0 (12 UTC 15 August 1999). $\mathcal{R}$ is a 2-dimensional circular domain of 300-km radius centered at the hurricane center, (i, j) represents model horizontal grid

12

points within $\mathcal{R}$ at the lowest σ level ($\sigma = 0.995$). The cost function J_{bgsat} was calculated over a 6-h window. The summation in (16) was carried out at t_n which represents the 12 observational times: $t_n = t_0 + \Delta t_n$, Δt_n=0, 46, 88, 107, 148, 167,208,226,268,287,328, and 346 minutes. The vector $\vec{r}_k$ represents the physical locations of all GOES-8 brightness temperatures at time t_n in domain B. Variables P and T_b represent the sea-level pressure and brightness temperature, respectively. J_b is a simple background term measuring the distance between the model state ($\mathbf{x}_0$) and the MM5 analysis based on the large-scale NCEP analysis ($\mathbf{x}_b$) . Both J_{bg} and J_{bgsat} are functions of the model initial condition $\mathbf{x}_0$. During the minimization procedure, $\mathbf{x}_0$ is adjusted to fit the model solution in the 6-h window to the bogus surface low and/or the GOES-8 brightness temperatures as closely as possible. W_P, W_{bt}, and W_b are diagonal weighting matrices approximating the error covariances of the bogus surface low, the brightness temperature data, and the background estimate of the model state, respectively. The value of W_P was considered simply as a constant and determined empirically by assuming a 1 hPa pressure error. W_{bt} was calculated based on the error statistics of the GOES-8 radiances. The brightness temperature error variance was computed by multiplying the radiance error variance (see eq. (10) and Table 2) by $(dT/dB)^2$, where dT/dB is the derivative of the temperature with respect to the Planck function. The value of W_{bt} is the inverse of the brightness temperature error variance Var. For the background term, the value of the weighting, W_b, was calculated as the inverse of the maximum differences at each vertical level of two MM5 analyses 12 hours apart.

All the data assimilation experiments were carried out on domain B (see below) at 30 km resolution using the adjoint modeling system of MM5 described by Zou et al. (1997) and Zou et al. (1998). The physical parameterizations included in the minimization program of the model were: a bulk aerodynamic formulation of the planetary boundary layer, a dry convective adjustment, grid-resolvable large-scale precipitation, and the Kuo cumulus parameterization scheme.

4.2   The forecast model

A version of the MM5 nonhydrostatic, movable, and triply nested grid model version was used for the 3.5 day numerical simulation of Hurricane Felix. The grid system contained the

triply nested meshes, 27 σ layers for all grid meshes with horizontal resolution of 90 km for the coarse domain A, 30 km for the intermediate domain B, and 10 km for the fine mesh domain C. The horizontal dimensions of domain A, B, and C were 45×51, 76×85, and 121×121, respectively (see Fig 2 in Zou and Xiao, 1999). Domains A and B were fixed throughout the simulation, while the 10-km domain C_i moved along the hurricane track, with domains C_1, C_2, C_3, and C_4 used for the forecast periods of 0-18 h, 18-42 h, 42-55 h and 55-84 h, respectively.

The model's moist processes included parameterization of shallow convection for all domains, Grell cumulus parameterization and stable precipitation scheme for domain A, Grell cumulus parameterization and Dudhia's simple ice explicit moisture scheme for domain B, and Kain-Fritsch cumulus parameterization and mixed-phase explicit moisture processes for domains C_1, C_2, C_3, and C_4. The high-resolution planetary-boundary layer parameterization scheme (Blackadar scheme) was used for all the domains. The land surface temperature was predicted using surface energy budget equations. For a more detailed description of MM5, see Dudhia (1993) and Grell et al. (1994).

4.3   Experiment design

We conducted four forecast experiments of 3.5 days duration, initialized at 12 UTC 15 August 1995. This is the time when Hurricane Felix was approaching the Outer Banks of North Carolina. The NHC (National Hurricane Center) official track forecast indicated that Felix would make a landfall in 72 h.

The same model configuration, described in section 4.2, was used for all the four forecast experiments. Only the initial conditions were different. The initial condition obtained by the standard preprocessing procedure of MM5 (Grell et al. 1994) was used as the initial condition for the control experiment (CTRL). The initial condition obtained with the use of surface bogus data through minimizing J_{bg} was used as the initial condition for the BG experiment. The initial conditions obtained with the use of both surface bogus data and satellite brightness temperature data through minimizing J_{bgsat} were used as the initial conditions for the BGSAT experiments. Only those GOES-8 brightness temperatures whose values differed from that of the large-scale analysis by less than 2 K were included in the data

14

assimilation procedures of BGSAT. The initial conditions on domain C_1 at 10-km resolution for the experiments BG and BGSAT were interpolated from that on domain B.

5   Numerical results from BDA with and without GOES-8 brightness temperatures

5.1   The Fit to data

In order to see how well the model fits to the GOES-8 brightness temperature data, we plot in Fig. 6 the means and the distances between the simulated and observed GOES-8 brightness temperatures for CTRL (dashed line), BG (dotted line), and BGSAT (solid line). The means and distances were calculated for all the GOES-8 observations available in the 6-h time window (from 12 UTC to 18 UTC 15 August 1995) that were included in the data assimilation procedures. The mean errors were reduced for all channels after data assimilation (Fig. 6a). Large error reductions in terms of distance of the analysis of BGSAT to the satellite observations occur mainly in the channels 5-8 and 10-15. As we know from the sensitivity study (Fig. 4), large sensitivities of the brightness temperatures at channels 5-8 and 13-14 are found in the low troposphere for both temperature and specific humidity fields. The brightness temperatures at channels 10-12 and 15 are more sensitive to the temperature and specific humidity in the mid and upper troposphere. The fit of the model state to observations at channels 9 and 16 are slightly degraded after data assimilation. The problem of the satellite data assimilation at channels 9 and 16 is found to be linked to the large observational error variances at these two channels (see the dash-dotted line in Fig. 6b). During the model fit to the specified bogus surface low, adjustments occurred outside the vortex region which resulted in the BG analysis being further away from the satellite data than the background field.

It is logical to expect error reductions of the model solution when comparing it with data that are assimilated. What will be the fit of the model forecasts of, say BGSAT, to observations that are not directly included in the assimilation procedure? For Hurricane Felix, we also had GOES-8 brightness temperature data during a 6-h period following the

15

data assimilation window. These were available at 10 time levels, with a total number of observations of 837, 140, 796, 148, 916, 151, 841, 106, 72 and 850 at 1846, 1928, 1947, 2028, 2047, 2129, 2147, 2229, 2328, and 2346 UTC 15 August 1995, respectively. The data at those times where the number of observations was less than 200 were found to be located in the northeast corner of the domain B, and data at other times (5 out of 10) covered the western half of the domain B. Since we were interested in assessing the impact of upstream conditions to the track prediction of Hurricane Felix, we calculated in Table 3 the fit of model forecasts to data at 1846, 1947, 2047, 2147, and 2346 UTC 15 August when the observations were located upstream and the number of observations were significantly larger (near or above 800). The brightness temperatures derived from the BGSAT model solution gave the

Table 3: The fit of the model forecasted state to GOES-8 brightness temperatures (the square-root of the distance between the simulated and observed T_b (unit: K))

experiment	T_b observational times					
	1846 UTC (837*)	1947 UTC (796)	2047 UTC (916)	2147 UTC (841)	2346 UTC (850)	total (4240)
CTRL	1.69	1.64	1.65	1.64	1.73	1.67
BG	1.61	1.59	1.57	1.52	1.63	1.59
BGSAT	1.56	1.54	1.55	1.57	1.67	1.57

*the number of observational points

best overall fit to the GOES-8 satellite data. It is encouraging to find that the fit of the BG forecast was generally slightly better than CTRL for the environmental flow prediction. Improvements in different channels for data at all the five time levels are shown in Fig. 7. Error reductions occurred for both BG and BGSAT for most channels during the entire 6-h forecast period. The error reduction in the BG forecast indicates a positive impact of the BDA generated hurricane on the prediction of environmental flow over the east coast and the eastern United States.

Model prediction contains errors of two types: errors in the initial condition and errors due to the imperfection of the forecast model. The fact that the forecast from BGSAT fits

the GOES-8 data better beyond the assimilation window indicates that important initial condition errors were corrected through satellite data assimilation and the improvement to the prediction of Hurricane Felix was felt beyond the assimilation window. These will be shown in greater details in the following two subsections.

5.2 Differences in the initial conditions with and without the use of GOES-8 brightness temperatures

As was mentioned in sections 2 and 3, GOES-8 brightness temperature information is directly sensitive to the atmospheric temperature and moisture fields. Figure 8 shows the mean and rms differences of the initial temperature and specific humidity fields between BGSAT and BG. The largest changes in the initial temperature field with the use of GOES-8 brightness temperature were near the surface and the top of the model (see solid line in Fig. 8b), with an increase of temperature near the surface (Fig. 8a). The relatively large changes in the temperature field near the model top, indicated by the rms difference, were found to be mainly over the vortex region. The mean and rms differences of the initial temperature fields between BGSAT and BG outside the vortex region (see the thick line circle in Fig. 5), shown in Fig. 8 as dash lines, confirm this. The largest change in the initial moisture field was at $\sigma = 0.75$ (model level 19, near 800 hPa), with a dry bias below the model level 14 and a small moist bias above it. Therefore, large changes to the initial condition describing the environmental flow outside the initial vortex region were mostly in the low levels for both the temperature and specific humidity fields. This implies either the model is better fitted to brightness temperatures at those wave bands that the brightness temperatures are most sensitive to, or the discrepancies between the background and observations at these wave bands are larger than other wave bands. The former appears to be the case if we combine the results in Figs. 4 and 6. The fit of the model state to observations was best achieved for the brightness temperatures in channels 5-14 (Fig. 6b, solid curve) and the maximum sensitivities for the brightness temperatures at most of these channels are in low troposphere (Fig. 4). The latter does not seem true since the fit of the CTRL analysis to the observations (dashed line in Fig. 6b) does not show an absolute peak at the wave bands of 5-8 and 10-15.

17

In what follows we first examine modifications made to the envionmental flow by the assimilation of the GOES-8 brightness temperatures, and then the differences of the initial vortices obtained in BG and BGSAT. Figure 9 shows the differences of the temperature at the surface (Fig. 9a) and the specific humidity at 850 hPa (Fig. 9b) between BGSAT and BG at the initial time. We find four major areas where temperature increase due to the inclusion of GOES-8 satellite data. The first is over the vortex region, the second in the western Atlantic (west of the vortex), the third near the Florida Penninsula, and the last one over the central Appalacians. The modification made to the background moisture field was mostly negative, indicating a reduced amount of moisture content after the assimilation. An elongated dry band is found to the west of the vortex. Comparing the surface temperature fields in BG and BGSAT (Fig. 10), we find that the two thermal ridges, one over the continent and the other over the ocean, are intensified after the assimilation of GOES-8 brightness temperatures. The enhanced thermal ridges as highlighted by 299 K and 300 K contours, reflect the temperature corrections to the initial condition as a direct result of adding satellite brightness temperature. This has the effect of building the thermal ridge over the Appalacians and to the west of storm. The cold air from the north was allowed to penetrate further south. The air to the west of storm is drier in the BGSAT by as much as 4 g kg^{-1} compared to that in BG (Fig. 11).

The low-level temperature increase was accompanied by changes in the wind fields through divergence flows generated by a downward motion responded to the surface temperature increase. For example, the regions of maximum increase of the surface temperature are found to be co-located with the centers of the maximum divergence near the surface (Fig. 12). A cross-section along a line AB in Fig. 12, cutting through the three maximum surface warming centers, shows that the temperature increase due to the fit to GOES-8 data was concentrated near the surface below 850 hPa (Fig. 13, thick solid lines). There was no significant temperature change above 850 hPa. However, a divergence center near the surface corresponds a convergence near the model top, with a descending motion (light shaded area) in the troposphere, and the corollary holds true (Fig. 13). These changes in wind fields were produced by the model constraint which responded to the temperature changes implied by the satellite brightness temperature information.

Although there were no satellite data over the vortex region at any instant in time, differences in the initial conditions over the vortex region with and without GOES-8 satellite data were resulted from the interaction of the bogused surface low and the background flow, the latter being modified by the satellite data. For example, the low-level wind ($\sigma = 0.995$) distribution in the BG vortex is different from the BGSAT vortex (Fig. 14). The maximum low-level wind in the BGSAT vortex was 53.6 m s^{-1}, which is much stronger than the maximum value of 36.7 m s^{-1} found in the BG vortex. The maximum low-level winds in the BGSAT initial condition were located to the north of vortex center, while they were located to the east-northeast of the vortex center in the BG. Differences arising from variation in the initial vortices of BG and BGSAT are also found in the other model fields (temperature, specific humidity, pressure perturbation and vertical velocity). Since their distributions are mostly axi-symmetric, we show in Fig. 15 a cross-section cutting through the initial vortex centers from the west to east (along line CD in Fig. 14). The BGSAT magnitude of adjustments in the temperature, specific humidity, pressure perturbation and vertical velocity show a realistic behavior than those from the BG assimilation. For example, the maximum temperature increase in the upper level of the BG vortex was as high as 26.3°C, while it was 14.7°C in the BGSAT vortex. The pressure increases in the upper level above the surface low were 11.8 hPa and 5.5 hPa for BG and BGSAT vortices, respectively. The vertical velocity on the east side of the BG vortex was greater than 600 cm s^{-1}, while it was 135 cm s^{-1} in the BGSAT vortex. A temperature adjustment of 26.3°C and a vertical velocity of 600 cm s^{-1} in BG are difficult to verify through observations. The temperature increase seems to be related to the adiabatic warming associated with the descent in the eye. In addition, the air in the eye of the initial BGSAT vortex was drier than that in the BG vortex. In summary, the hurricane eye and the eye-wall were generated in both BDA experiments, with descending, warm and dry air in the center of the hurricane and ascending moist air around the eye throughout the entire layer of the model atmosphere. However, the BGSAT vortex seems to be quantitatively more realistic than that of the BG vortex.

Seeing the differences in both the environment flow and the initial vortex described by the BG and BGSAT initial conditions, one compelling question would be what impact these differences have on the forecasts? Or are they significant to make a difference in the 2 to 3.5

day prediction of Hurricane Felix? Results of the three model predictions using the NCEP analysis (CTRL), the BG initial condition, and the BGSAT initial condition, are shown in the following section. Emphasis is placed on comparing numerical forecast results from BG and BGSAT.

6 Impact of Satellite data on the prediction of Hurricane Felix

As mentioned before, the bogus and satellite data assimilation experiments were carried out on a single domain B at 30-km resolution over a half hour (for BG) and 6-h (for BGSAT) window, respectively. The initial conditions on domain C at 10-km resolution were obtained from the initial conditions at 30-km by a linear interpolation. The initial condition for domain A at 90-km was the NCEP large-scale analysis. Once the three sets of initial conditions for CTRL, BG, and BGSAT were obtained, three 84-h (3.5 days) model simulations were carried out using the same model configuration as described in section 4.2.

The impact of satellite data on the track and intensity forecast of Hurricane Felix is first assessed by comparing the observations with the predicted hurricane positions, the values of the central sea-level pressure and the maximum low-level wind. Figures 16 and 17 show the track and intensity change at 6-h intervals for the entire forecast period from 12 UTC 15 August to 00 UTC 19 August 1995. The forecast with a cold start without data assimilation (CTRL) did reasonably well for the track prediction during the initial 36 h. However, It failed to predict a north eastward recurving movement of the simulated hurricane. The forecasts with bogus data and/or satellite data assimilation (BG and BGSAT) produced a much improved prediction of the recurvature and the subsequent eastward movement that occurred between 42-76 h. The BGSAT forecast performed similarly to that of the BG forecast for the hurricane track before 42 h of model integration. After 42 h, the hurricane track in BGSAT was closer to the observed and better than BG. This difference in performance was found to be related to the differences in the prediction of the upper-level jet (near 200 hPa) between BG and BGSAT, with the satellite data showing a beneficial impact in the upper-level jet

20

prediction (shown later). The hurricane tracks in both BG and BGSAT before 42 h were located to the east of the observed track. Further study is needed to identify the possible cause.

The central SLP and maximum low-level wind were predicted similarly well by BG and BGSAT (see Table 4), except that during the initial 6 hours, BG experienced a spin-up

Table 4: Errors of the 3.5 day forecast of Hurricane Felix

experiment	track		central SLP		low-level maximum wind	
	mean	distance	mean	distance	mean	distance
CTRL	152	197	34	34	-15	16
BG	45	50	-3	5	4	4
BGSAT	40	46	0	3	4	3

time in the value of SLP and BGSAT had a stronger maximum low-level wind at the initial time. The SLP predicted by BG and BGSAT at 18 UTC 15 August 1999 (the first 6-h model integration) was 952 hPa and 968 hPa, compared with the observed value of 966 hPa. In addition, the BG is characterized by an extremely large amount of precipitation that occurred at the initial time. The 6-h accumulated rainfall was 375 mm in BG, but was substantially reduced to 174 mm in BGSAT. Another noticeable feature in the intensity forecast is that the simulated hurricane in BGSAT is consistently weaker than that of BG during the entire forecast period.

Hurricane Felix made its northward turning from its northwest track between 18 UTC 16 and 06 UTC 17 August 1995, and northeastward and then eastward track after 06 UTC 17 August 1995. There was an upper-level environmental anticyclonic flow (near 200 hPa) and a low-level synoptic cold front near the east coast of the United States that prevented Hurricane Felix from continuing its northwest track, which could have resulted in a landfall.

The difference in the track prediction that occurred around 42-48 h (6-12 UTC 17 August) between BG and BGSAT might be related to several factors: (i) the difference in the intensity of the upper-level jet, (ii) the location of maximum latent heat release around the hurricane eye, and (iii) the vertical structure of the simulated Hurricane Felix. Figure 18 shows, for

example, the upper-level wind ($\sigma = 0.025$, model level 2, near 200 hPa) from BG (right panels) and BGSAT (left panels) simulations at 1200 UTC 17 August 1995 for domain A. We find that the westerly jet west of Hurricane Felix in BGSAT was much stronger than that in BG (Fig. 18 c and d). The maximum wind in BGSAT at 12 UTC 17 August 1995 was 28.2 m s^{-1} and was located closer to the hurricane center. The maximum wind in BG was 23.5 m s^{-1} and was located much further west and away from the center. We also noticed that the hurricane is located in the left jet exit region in BGSAT and the BG hurricane was located to the east of jet tip. The upper-level westerly jet was resulted from the large-scale environmental response to the anticyclonic flow that fanned out of the hurricane center and came all the way from east, south, west and northward around the immediate environment of the hurricane. The stronger jet in BGSAT was found to be related to the stronger southerly flow that developed between 00 UTC 16 August and 00 UTC 17 at the south and southwest of the hurricane (Fig. 18 a and b). The latter is related to the low-level temperature and moisture changes that resulted from the satellite data assimilation, which extended to upper-level during the course of model integration. Figure 19 shows the temperature distributions at model level 11 ($\sigma = 0.43$, Fig. 19a) and 27 ($\sigma = 0.995$, Fig. 19b) and moisture distribution at 850 hPa (Fig. 19c) on domain A for both BG and BGSAT at 18 UTC 16 August 1995. We find that the cold trough in the upper troposphere (Fig. 19a) was stronger in BGSAT than in BG. This was found at all the model levels from 9 ($\sigma = 0.35$) to 14 ($\sigma = 0.55$). Near the surface, major differences between BGSAT and BG are that (i) the upstream thermal ridge west of the surface cold front in BGSAT was stronger than that in BG, and (ii) the air in the immediate vicinity of the hurricane was drier in BGSAT than in BG. The differences in the environmental temperature distribution, whose difference pattern is elongated in the north and south direction, increase the thermal gradient of the layer-averaged temperature in the direction from west to east and thus, increase the meridional wind component (see Fig. 18) based on the thermal wind relation.

We notice that the cooler and drier air started to wrap from the west and southwest of the hurricane at about 18 UTC 16 August 1995 in BGSAT (Fig. 19b), which was delayed to 00 UTC 17 in the BG simulation (figure omitted). The cooler air that wrapped from the west and south of the hurricane in BGSAT was drier than that in BG (see Fig. 19c).

Differences in the predictions of hurricane structures between BG and BGSAT were also found in the location of maximum rainfall and maximum rainwater distributions, and the size of the hurricane eye reflected in the hurricane cloud pictures or rainfall distributions. An example is shown in Fig. 20 which plots the vertically integrated hydrometeor fields at 18 UTC 16 August 1995. The maximum vertically integrated hydrometeor fields in BGSAT at various times were found to be located mostly to the north of the hurricane center during the recurving period (18 UTC 16 to 18 UTC 17 August 1995, see Fig. 20). In the BG forecast, it was located to the east or slightly east-northeast of the simulated hurricane center. The 6-h rainfall patterns showed a similar feature. The simulated hurricane eye in BGSAT was larger than that in BG during the entire forecast period of 3.5 days. Such a difference in the meso-convective scale precipitation and cloud distributions explain the difference in the hurricane intensity forecasts (see Fig. 17a) between BG and BGSAT. The smaller hurricane eye permits the high angular momentum low-level flows to advance closer toward the storm's center than a larger-eye hurricane would (Krishnamurti et al. 1998a, b), resulting in a stronger intensity forecast as in the case of BG. This is confirmed by the differences between BG and BGSAT of the central SLP values during the entire forecast period (Fig. 17a). We believe that the latent heat release associated with these moisture processes contributed to the larger northward component in the BGSAT hurricane track prediction after 18 UTC 16 August. The BGSAT hurricane was track located further north than the BG hurricane track (see Fig. 16), as was in reality.

The difference in the regions of maximum convection may be associated with the differences in upper-level jet intensity mentioned before. An interesting difference between BG and BGSAT is in the vertical structure of hurricane Felix. Before 18 UTC 16 August, the warm center coincided with the hurricane SLP center and the cyclonic circulation around the eye at all vertical levels in both BG and BGSAT. After 18 UTC 16 August, the warm center at the upper-level (near 200 hPa) and the low-level near the surface, no longer coincided with the cyclonic circulation centers at all levels in BGSAT. The warm anomaly and the circulation center were co-located only between 300 hPa and 850 hPa, and not at other levels. Figure 21 presents the streamline, the temperature, and the wind barbs at 200 hPa at 18 UTC 16 and 06 UTC 17 August 1999. At 18 UTC 16 in BG, the cyclonic circulation at 200 hPa

coincided with the low-level hurricane center (indicated by a star sign), and the warm center was slightly behind the hurricane circulation center (Fig. 21a). In the BGSAT prediction, the upper-level cyclonic circulation center was not co-located with the warm center nor with the SLP center but shifted to the northeast (Fig. 21b). Similar features were found at 00 UTC 17 (Figures omitted). At 06 UTC 17, the BG upper-level circulation center had moved to the northeast of the low-level hurricane center and was co-located again with the warm center (Fig. 21c), while in BGSAT, the upper-level circulation center continued to be ahead of the low-level hurricane center and the maximum temperature center (Fig. 21d). After 12 UTC 17, the hurricane circulation resumed its vertical alignment with the maximum temperature center still lagging behind the circulation center (Figures omitted). The eastward shift of the temperature maximum center from low levels to upper levels is believed to be resulted from the stronger eastward temperature advection in BGSAT than in BG due to the stronger upper-level jet in BGSAT. This increased upper-level jet contribution to an increased vertical shear in BGSAT. The upper-level cyclonic circulation, which was located to the north of the maximum temperature center, is a result of jet dynamics. The cyclonic circulation usually appears in the left jet exit region.

7   Summary and conclusions

The influence of satellite data on the prediction of Hurricane Felix has been evaluated by comparing the MM5 model integrations with and without including the satellite data in the BDA hurricane initialization procedure. All model integrations were performed for 84 hours, each beginning at 12 UTC 15 August 1995 before the Felix storm made its recurvature from its northwest track. This experimental design allowed the examination of Hurricane Felix making its north and northeast turning during 18 UTC 16 to 18 UTC 17 August 1995. If Hurricane Felix continued its northwest movement, it would have made landfall at the North Carolina coast. The differences between the forecasts with and without satellite data represented the satellite influence.

An observation operator that links the atmospheric state to the GOES-8 brightness temperatures and the adjoint of the observation operator were developed and linked to the

MM5 adjoint model system. The GOES-8 satellite data were then included in a hurricane initialization scheme, the BDA scheme using a bogus surface low. Whilst the bogusing of a surface low alone improved the description of the dynamic and thermodynamic structures of the initial vortex and the subsequent hurricane track and intensity prediction, the inclusion of satellite brightness temperature data in BDA were found to be influential and beneficial for the hurricane initialization and forecast. Several changes occurred to the thermodynamic and synoptic description of the low-level environmental fields at the initial time, including an intensified low-level warm ridge to the west of the hurricane, a decreased amount of water vapor below 500 hPa over most areas where satellite data were available, and an intensified warm synoptic ridge over the U. S. continent. Even though there were no cloud-free satellite data over the region of initial vortex, differences between the initial vortices with and without the use of GOES-8 brightness temperature data were identified, generating a conceptually more realistic vortex structure when satellite data were included than the one obtained using only the bogus data.

Impacts of the satellite data on the hurricane prediction were reflected in several aspects of the forecast. The track forecasts during the northeast turning of Hurricane Felix was slightly improved when satellite data were included in the initialization procedure. Differences in the prediction of Hurricane Felix with and without satellite data were also found in the prediction of the central SLP, the upper-level jet, and the cold front which prevented Hurricane Felix from continuing its west-northwest track at 18 UTC 16 August 1995. As a result of stronger temperature trough-ridge structures ahead of the hurricane, the upper-level jet to the west of the hurricane around 12 UTC 17 August predicted with the use of satellite information was much stronger than other predictions without using satellite data. The stronger temperature advection and the modification to the location of the maximum rainfall and cloud distributions contributed to the larger northward movement component of Hurricane Felix's track before the eastward turning of the track.

This study identified changes in the prevailing environment through the direct use of GOES-8 satellite brightness temperature data in a single data assimilation experiment. The modified environment in turn influences the storm motion, the intensity, the structure of the storm, and the rainfall. These results represent an example showing the potential impact of

environmental satellite data on the hurricane prediction. The specific differences shown here may vary from case to case and are likely to depend on the particular large-scale environment as well as the hurricane location, size, and structure. However, several features influenced by satellite data, such as improved low-level temperature and moisture initial fields, a more realistic 3-dimensional dynamic and thermodynamic structure of the initial vortex, and the positive impact on the prediction, are likely to be found in other cases as well. Although, some of the changes in the predictions with and without satellite data seem to be marginal, more significant impact can be expected with the use of much more satellite data in a cycling data assimilation mode.

8 References

Andersson, E., J. Pailleux, J-N. Thepaut, J. R. Eyre, A. P. McNally, G. A. Kelly, and P. Courtier, 1992: Use of radiance in 3D/4D variational data assimilation. Proceedings of a workshop held at ECMWF on variational assimilation, with special emphasis on three-dimensional aspects, 9-12 December 1992, European Centre for Medium-Range Weather Forecasts, Reading, U.K., 123-156.

Clough, S. A., M. J. Iacono, and J.-L. Moncet, 1992: Line-by-line calculation of atmospheric fluxes and cooling rates: Application to water vapor. *J. Geophys. Res.*, **97**, 15,761-15,785.

Derber, J. C. and W. S. Wu, The use of TOVS cloud-cleared radiances in the NCEP's SSI analysis system, *Mon. Wea. Rev.*, **126**, 2287-2299, 1998.

Dudhia, J., 1993: A nonhydrostatic version of the Penn State-NCAR mesoscale model: Validation tests and simulation of an Atlantic cyclone and cold front. *Mon. Wea. Rev.* **121**, 1493-1513.

Eyre, J. R, 1991: A fast radiative transfer model for satellite sounding systems, Research Department Technical Memorandum No. 176, ECMWF, 28pp.

Eyre, J. R., G. A. Kelly, A. P. McNally, E. Andersson and A. Persson, 1993: Assimilation of TOVS radiance information through one-dimensional variational analysis. Quart. J. Meteorol. Soc., **119**, 1427-1463.

Eyre, J. R., and H. M. Woolf, 1988: Transmittance of atmospheric gases in the microwave region: A fast model. Appl. Opt., 27, 3244-3249.

Fleming, H.E., N.C. Grody, and E.J. Kratz, 1991: The forward problem and corrections for the SSM/T satellite microwave temperature sounder. IEEE Transactions on Geoscience and Remote Sensing, 29:4, 571-583.

Grell, G. A., J. Dudhia, and D. R. Stauffer, 1994: A description of the fifth-generation Penn State/NCAR mesoscale model (MM5). *NCAR Technical Note*, NCAR/TN-398 + STR, National Center for Atmospheric Research, Boulder, CO, 138 pp.

Hillger, D. W., and T. H. Vonder Haar, 1988: Estimating moise levels of remotely sensed measurements from satellites using spatial structure analysis. *J. Atmos. Oceanic Tech.*, **5**, 206-214.

Hollinger, J. P., 1991: DMSP Special Sensor Microwave/Imager Calibration/Validation. Final Report Vol. II, Naval Research Laboratory, Washington D. C., 12-25.

Karyampudi, V. Mohan, G. S. Lai, and J. Manobianco, 1998: Impact of initial conditions, rainfall assimilation, and cumulus parameterization on simulations of Hurricane Florence (1988). *Mon. Wea. Rev.*, **126**, 3077-3101.

Krishnamurti, T. N., W. Han, and D. Oosterhof, 1998a: Sensitivity of hurricane intensity forecasts to physical initialization. *Meteorol. Atmos. Phys.*, **65**, 171-181.

Krishnamurti, T. N., W. Han, B. Jha and H. S. Bedi, 1998b: Numerical simulation of Hurricane Opal. *Mon. Wea. Rev.*, **126**, 1347-1363.

Krishnamurti, T. N., S. K. Roy Bhowmik, D. Oosterhof, and G. Rohaly, 1995: Mesoscale signatures within the tropics generated by physical initialization. *Mon. Wea. Rev.*, **123**, 2771-2790.

Lion, K-N, 1980: An Introduction to Atmospheric Radiation, Academic press, New York.

Lipton, A.E., 1998: Improved GOES sounder coverage of cloud-broken data fields. J. Appl. Meteor., 37, 441-446.

Menzel, W. P., and J. F. W. Purdom, 1994: Introducing GOES-I: The first of a new generation of Geostationary Operational Environmental Satellites. Bull. Amer. Met. Soc., 75, 757-781.

Peng, M. S., and S. W. Chen, 1996: Impacts of SSM/I retrieved rainfall rates on numerical prediction of a tropical cyclone. *Mon. Wea. Rev.*, **124**, 1181-124.

Smith, E. A., and T. F. Lee, 1995: Seventh conference on satellite meteorology and oceanography. Bull. Amer. Met. Soc., 76, 363-371.

Xiao Q., X. Zou, and Y.-H. Kuo, 1999: Incorporating the SSM/I Derived Precipitable Water Vapor and Rain Rate into a Numerical Model: A Case Study for ERICA IOP-4 Cyclone. *Mon. Wea. Rev.*, (accepted)

Zou, X., A. Barcilon, I. M. Navon, J. Whitaker, and D. G. Cacuci, 1993: An adjoint sensitivity study of blocking in a two-layer isentropic model. *Mon. Wea. Rev.*, **121**, 2833-2857.

Zou, X., W. Huang, and Q. Xiao, 1998: A user's guide to the MM5 adjoint modeling system. NCAR Technical Note, 1997, NCAR/TN-437+IA, pp92.

Zou, X., Y.-H. Kuo, and Y.-R. Guo, 1995: Assimilation of atmospheric Radio Refractivity Using a Nonhydrostatic Adjoint Model. *Mon. Wea. Rev.*, **123**, 2229-2249.

Zou, X., F. Vandenberghe, M. Pondeca, and Y.-H. Kuo, 1997: Introduction to adjoint techniques and the MM5 adjoint modeling system, *NCAR Technical Note*, NCAR/TN-435 - STR, National Center for Atmospheric Research, Boulder, CO, 110pp.

Zou, X., and Q.-N. Xiao, 1999: Studies on the initialization and simulation of a mature hurricane using a variational bogus data assimilation scheme. *J. A. S.*, (accepted)

9 CAPTIONS

Fig. 1: (a) The GOES-8 infrared cloud image at 2346 UTC 15 August, and (b) the distributions of the GOES-8 observed brightness temperatures at 00 UTC 16 August 1995. The numbers in Fig. 1b are the differences between the NCEP analysis-derived and GOES-8 observed brightness temperatures at sounder channel 8 (11.03 μm) at 00 UTC 16 August 1995. Positive numbers indicate the observed values are smaller than the computed values. Cloudy data have been excluded from (b).

Fig. 2: NCEP sea-level pressure analysis enhanced by MM5 pre-processing procedure at 1200 UTC 15 August 1995. The stars indicate locations at which the adjoint sensitivities of the GOES-8 brightness temperatures were calculated.

Fig. 3: Relative sensitivities of the brightness temperatures at (a-b) channel 6 (12.66 μm) and (c-d) channel 11 (7.02 μm) with respect to temperature (left panels) and humidity (right panels) profiles located at the eight points indicated in Fig. 2 (thin solid line). The averaged profiles are shown as the thick dashed lines.

Fig. 4: Averaged relative sensitivities of the brightness temperatures at all the 18 channels with respect to temperature (solid lines) and humidity (dashed lines) profiles. The average is taken on all the eight selected points.

Fig. 5: Locations of all the brightness temperature observations (dots) that were available over the model domain B for assimilation. The thick iso-lines show the distribution of the bogused sea-level pressure of the initial hurricane vortex.

Fig. 6: (a) Mean differences and (b) distances of all the brightness temperatures in the assimilation window derived from CTRL (dashed line), BG (dotted line), and BGSAT (solid line) to GOES-8 satellite observations. Also shown in (b) are the observational error variances at different channels (dash-dotted line in Fig. 6b).

Fig. 7: Distances of the brightness temperatures at all channels at the five time levels where the number of observations was large and close to 800 in the 6-h forecast from 1800 UTC 15 August 1995.

Fig. 8: The mean (left panel) and distance (right panel) of the initial differences in the (a-b) temperature and (c-d) specific humidity fields between BGSAT and BG. Solid lines are for all domain B and dashed lines are only for the hurricane vortex region defined in Fig. 5.

Fig. 9: Differences in the initial conditions of the (a) temperature at the surface and (b) specific humidity at 850 hPa between BGSAT and BG. The contour intervals are 1° C for the temperature and 1 g kg^{-1} for the specific humidity.

Fig. 10: Distributions of the initial temperature fields from (a) BG and (b) BGSAT. The contour interval is 1 K. The two thick lines are for the temperature at 299 K and 300 K.

Fig. 11: Distributions of the initial specific humidity fields from (a) BG and (b) BGSAT. The contour interval is 1 g kg^{-1}. The thick line is for the specific humidity of 9 g kg^{-1}.

Fig. 12: Distributions of the differences in the initial temperature (thick lines) and divergence (shaded areas for the divergences greater than 5 $\times 10^5$ s^{-1}) fields between BG and BGSAT. The contour interval for the temperature is 1 K.

Fig. 13: Cross-sections of the differences of the temperature (thick lines), vertical velocity (dark shaded areas for the vertical velocity greater than 5 cm s-1 and the light shaded areas for the vertical velocity less than -5 cm s-1) fields between BGSAT and BG along the line AB in Fig. 12.

Fig. 14: Distributions of the low-level wind ($\sigma = 0.995$) of the (a) BG vortex and (b) BGSAT vortex. The contour intervals is 5 m s^{-1}.

Fig. 15: Cross-sections of the adjustment of initial temperature in (a) BG and (b) BGSAT, and the adjustment of initial specific humidity in (c) BG and (d) BGSAT. The cross-sections are oriented through the initial vortex centers from the west (left) to east (right). The temperature and specific humidity intervals are 2 K and 2 g kg^{-1}, respectively. Light shading area represents the downward motion where the vertical velocity was less than -15 cm s^{-1} and the dark shading area represents the upward motion where the vertical velocity was larger than 15 cm s^{-1}.

Fig. 16: (a) Hurricane track at 6-h interval for the entire forecast period from 1200 UTC 15 August to 00 UTC 19 August 1995. (b) The track position error (km) in the 84-h

forecast beginning at 1200 UTC 15 August 1995. (The circle sigh represents for CTRL, asterisk for BG, and square for BGSAT. The dot sign represents observation)

Fig. 17: 84-hour variations of (a) Sea-level pressure (hPa) and (b) Maximum low-level wind speed (m s^{-1}) beginning at 1200 UTC 15 August 1995. (the dot sign for the observation, circle for CTRL, asterisk for BG and square for BGSAT).

Fig. 18: Simulations of upper-level wind barbs and isotach (thick line with 5 m s^{-1} interval) at $\sigma = 0.07$ (approximately 200 hPa) for domain A from experiment (a) BGSAT and (b) BG at 1800 UTC 16 August 1995, and from experiment (c) BGSAT and (d) BG at 1200 UTC 17 August 1995. The shaded area shows the wind speed larger than 20 m s^{-1} in (a) and (b), and larger than 15 m s^{-1} in (c) and (d). The hurricane symbol represents the predicted sea-level pressure center of the hurricane at the corresponding time, and by the corresponding experiment.

Fig. 19: Temperature fields predicted by BGSAT (thick line with 1 K interval) and the temperature difference fields between BGSAT and BGSAT (light shading area with dashed perimeter for negative values less than -0.25 K, dark shading area with solid perimeter for positive values larger than 0.25 K) at 1800 UTC 16 August 1995 at (a) $\sigma = 0.43$ and (b) $\sigma = 0.995$. The surface wind vectors are shown in Fig. 19b. (c) 850-hPa specific humidity fields predicted by BGSAT (thick line with 1.0 g kg^{-1} interval) and the specific humidity difference between BGSAT and BG (light shading area with dashed perimeter for negative values less than -0.5 g kg^{-1}) dark shading area with solid perimeter for positive values larger than 0.5 g kg^{-1}) at 1800 UTC 16 August 1995.

Fig. 20: Vertically integrated model hydrometeors (shading in scale, unit: mm) and sea-level pressure (thick line, 5-hPa interval) at 1800 UTC 16 August 1995 by (a) BG and (b) BGSAT. The heavy dots represent the centers of the maximum hydrometeors which are linked to the hurricane centers (represented by the hurricane symbol) through thin straight lines. The labels beside the heavy dots represent the times.

Fig. 21: 200-hPa wind barbs, streamlines, and temperature analysis (thick line at 0.5 K interval) from BG (left panels) and BGSAT (right panels) at 1800 UTC 16 August 1995 for (a) and (b), and at 06 UTC 17 August 1995 for (c) and (d). The star sign represents

the sea-level pressure center of Hurricane Felix predicted by BG (in left panels) and BGSAT (in right panels).
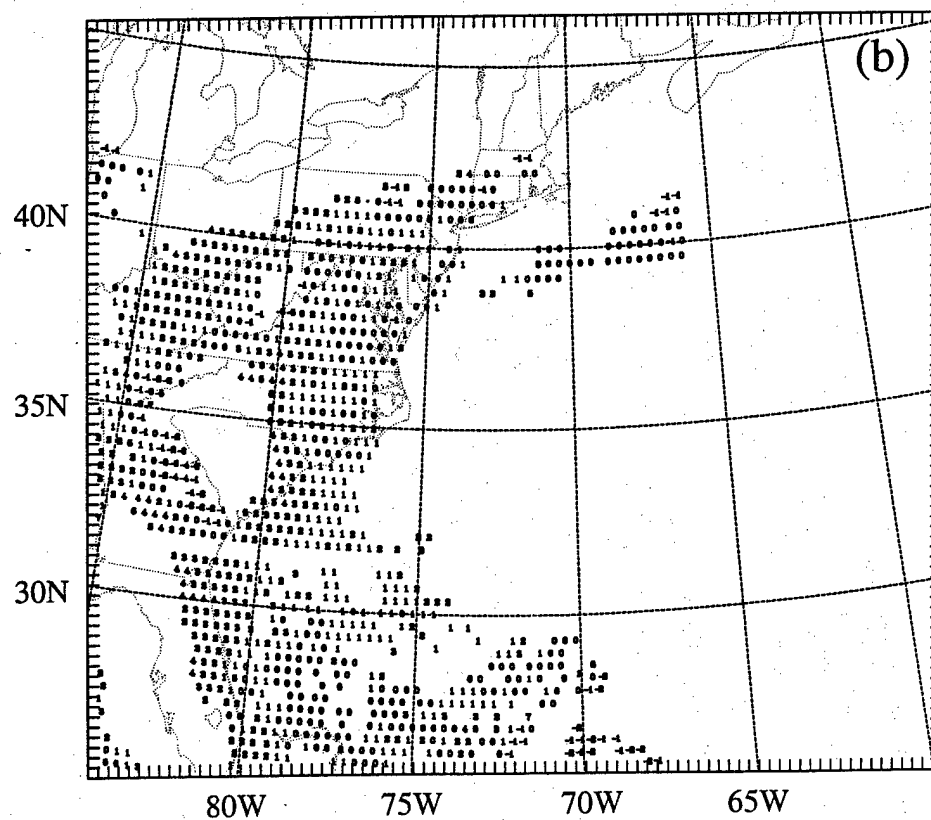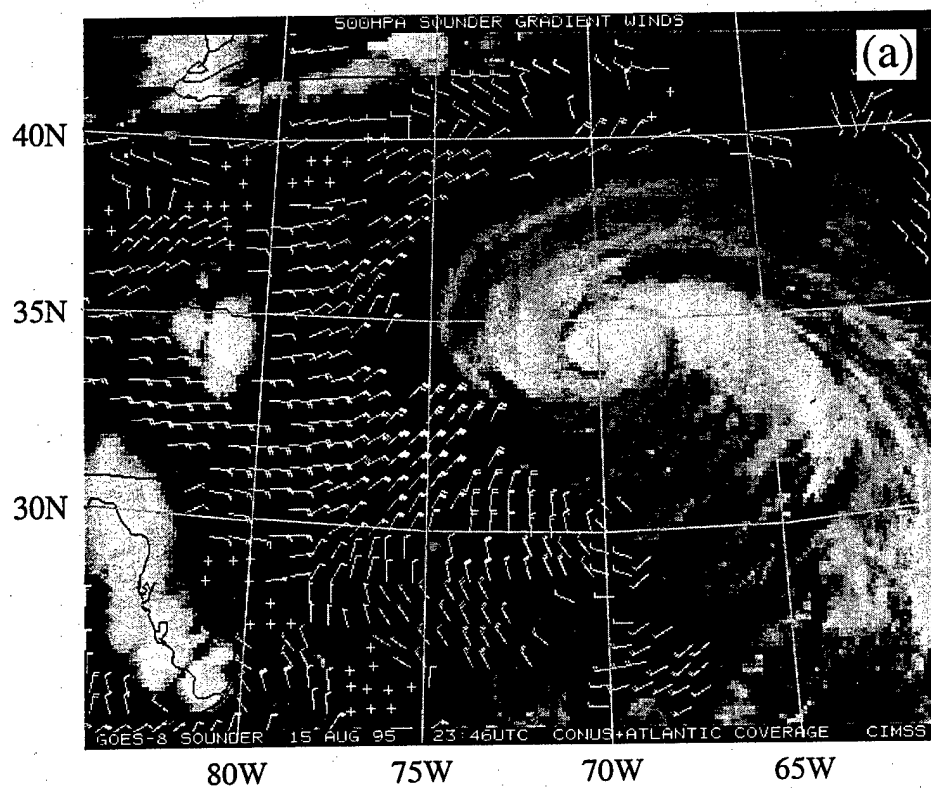
Fig. 1
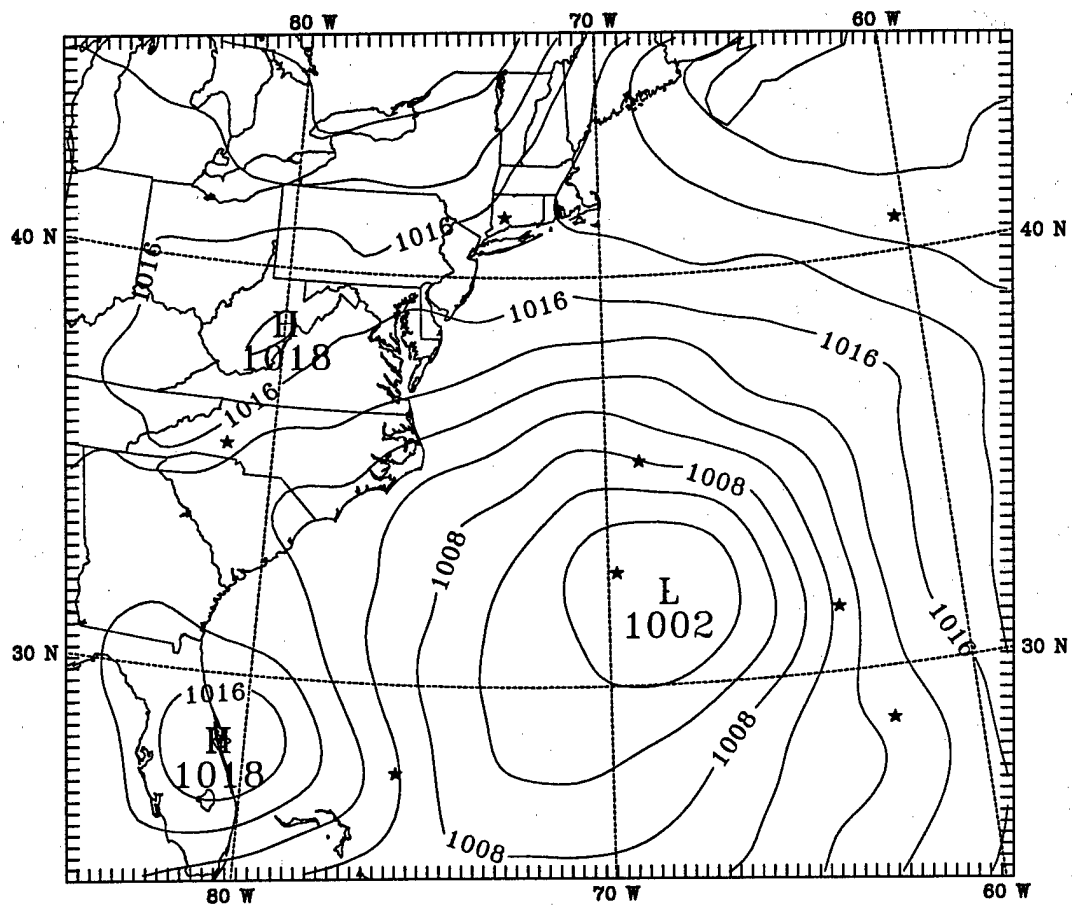
Fig. 2
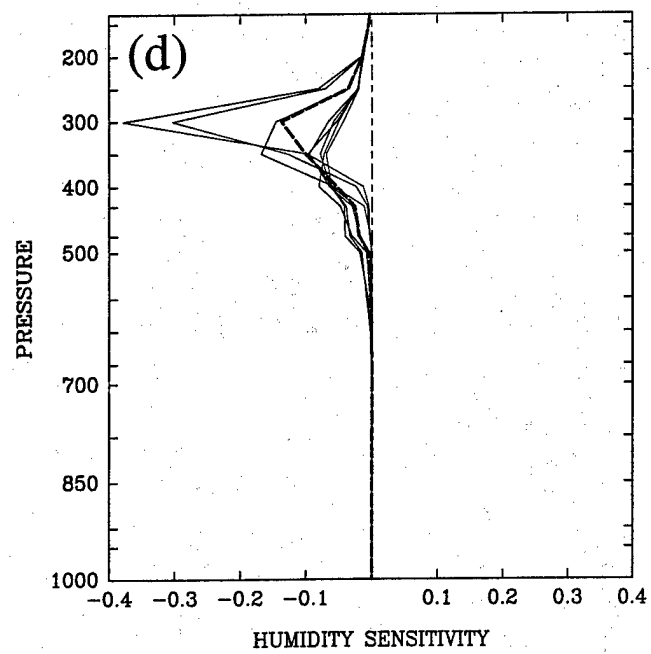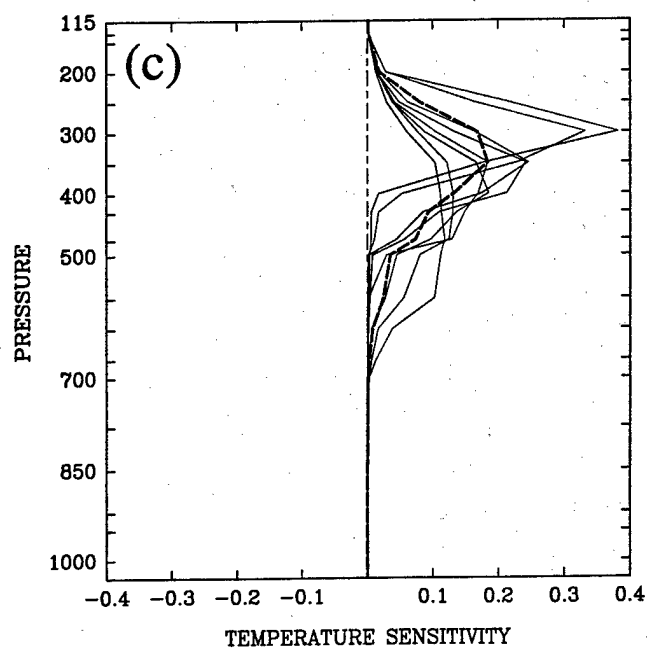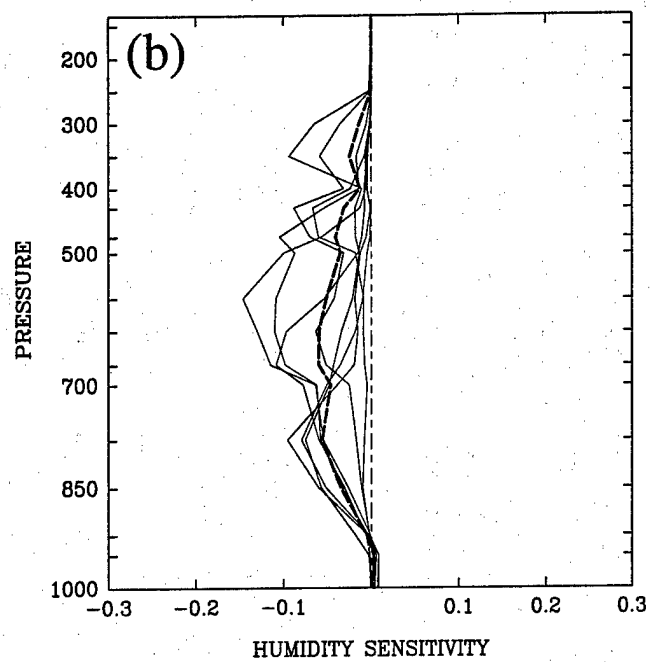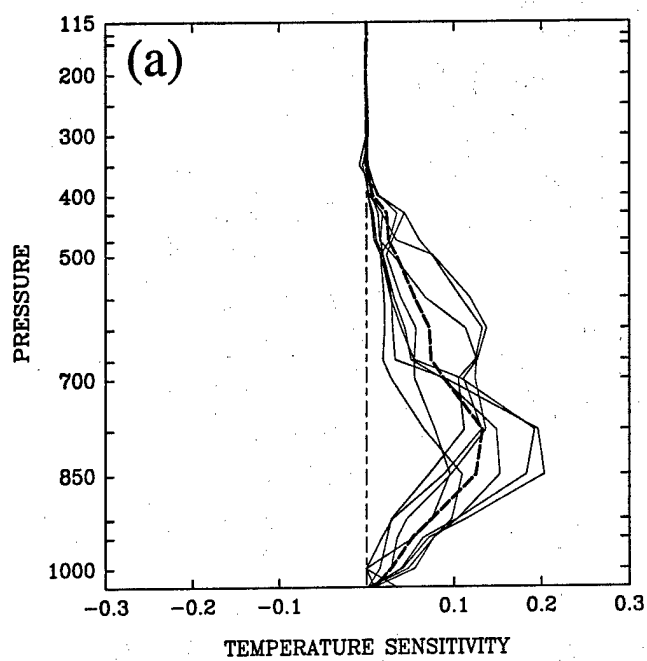
Fig. 3
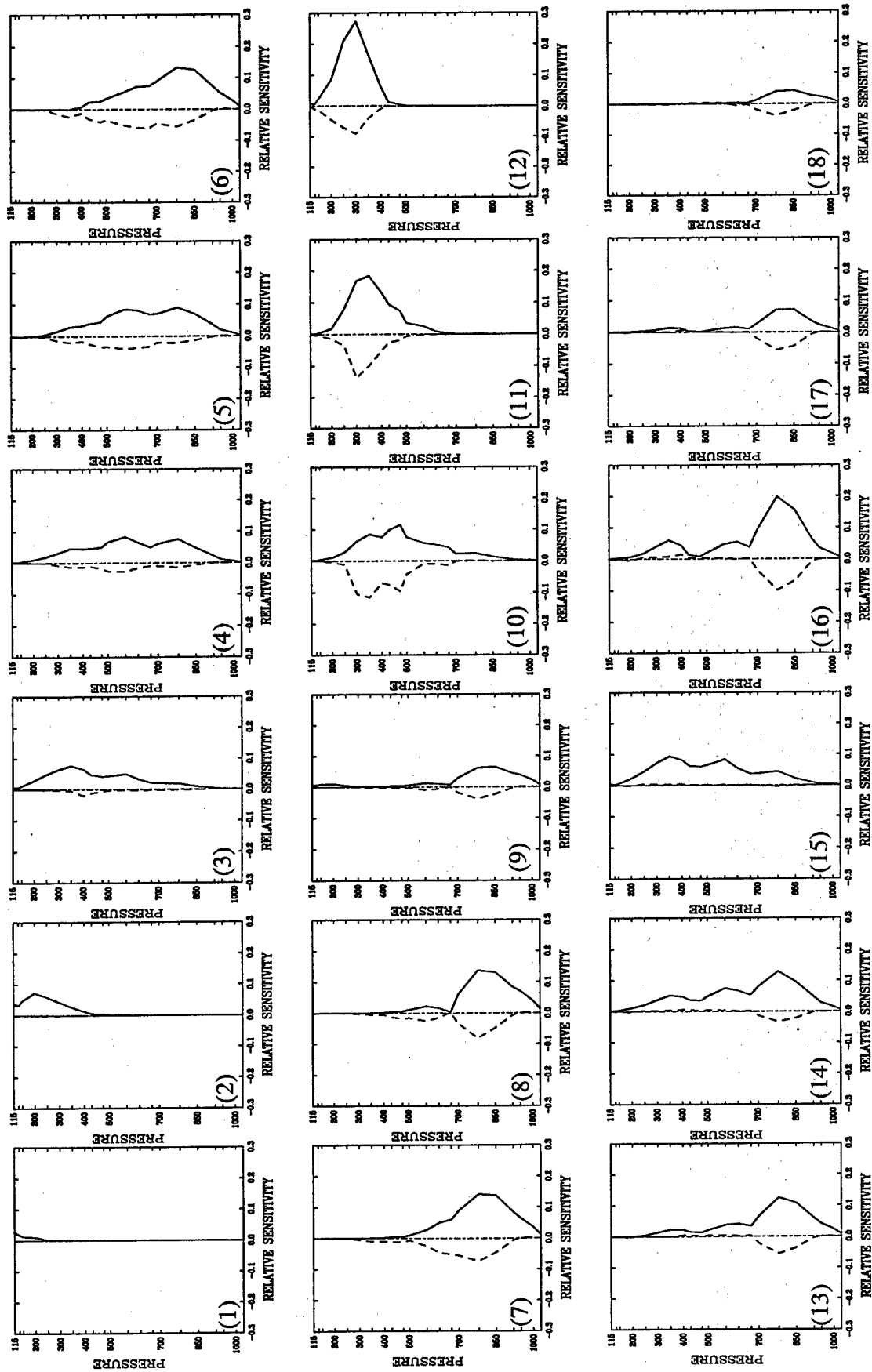
Fig. 4
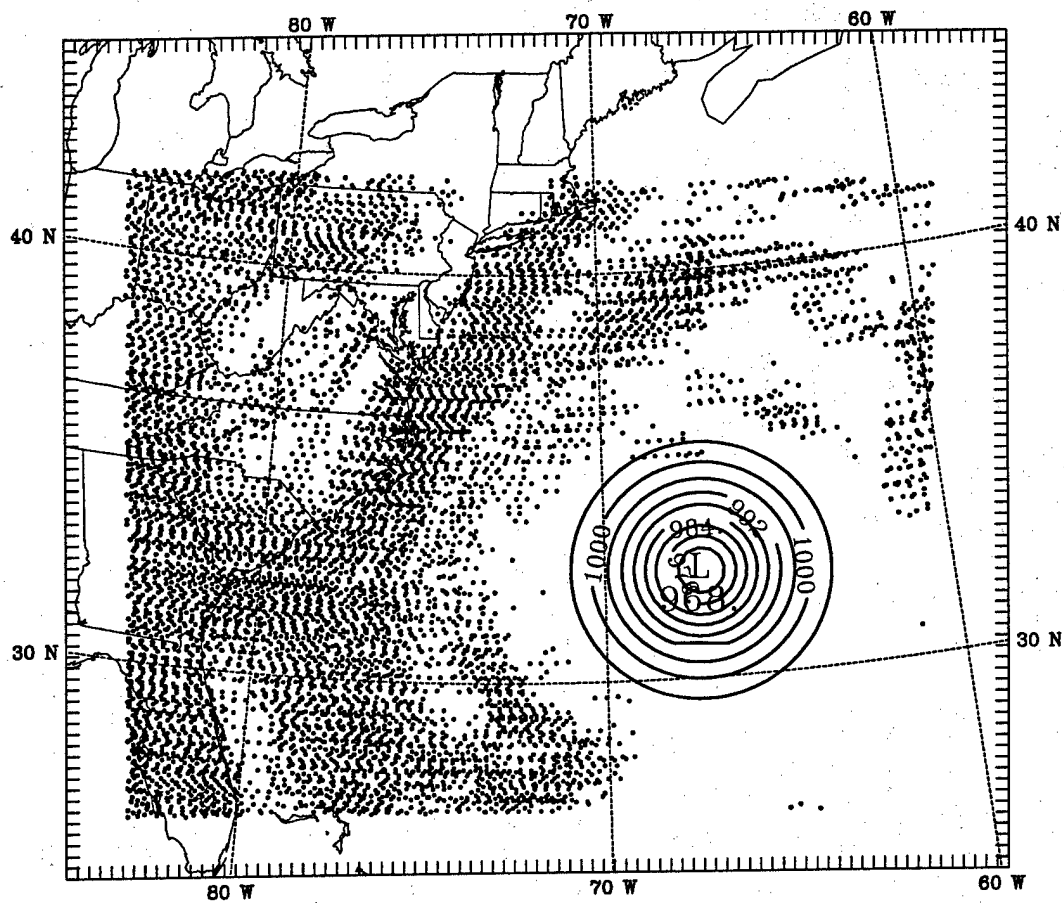
Fig. 5
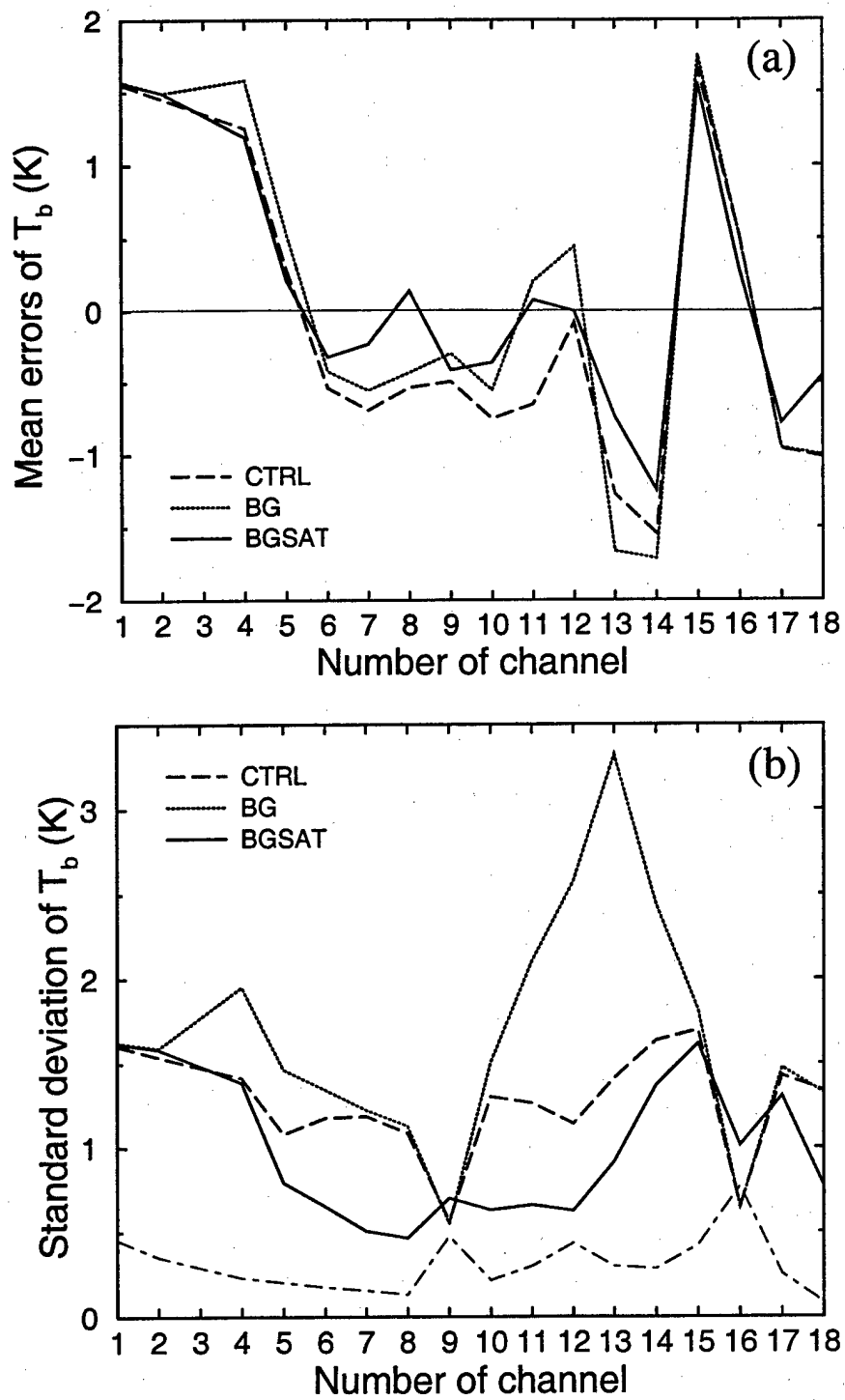
Fig. 6
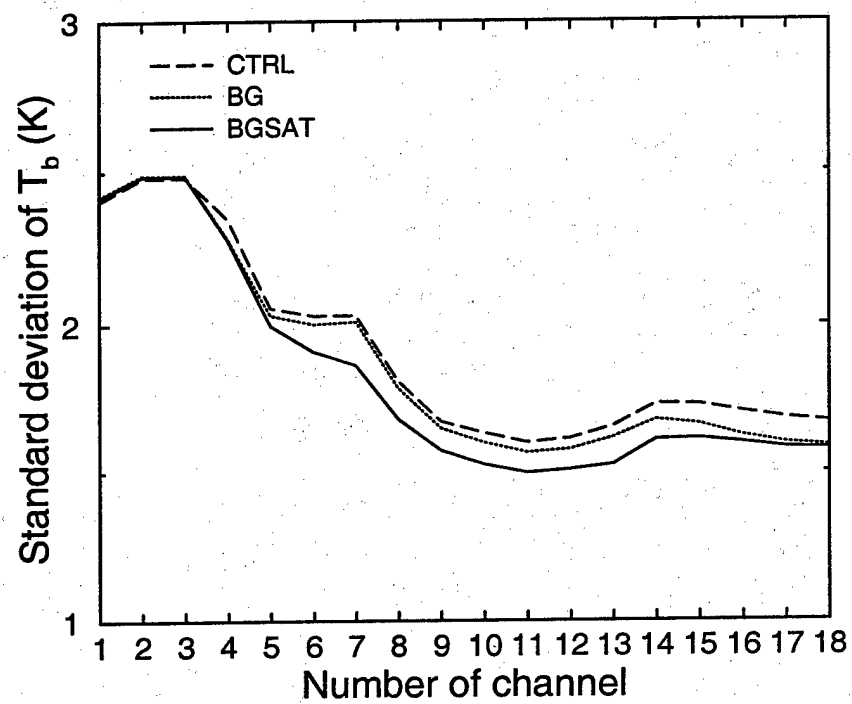
Fig. 7
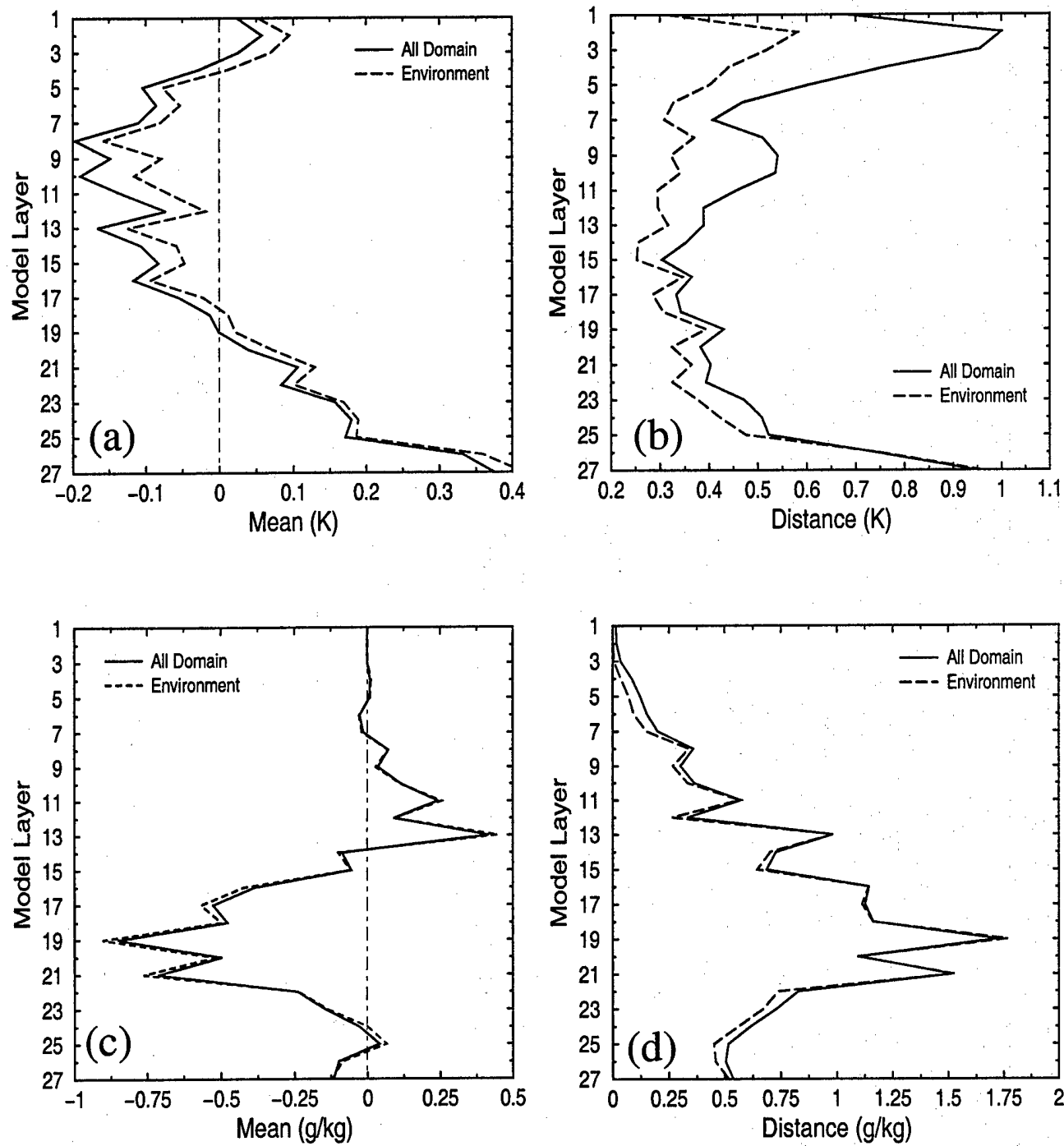
Fig. 8
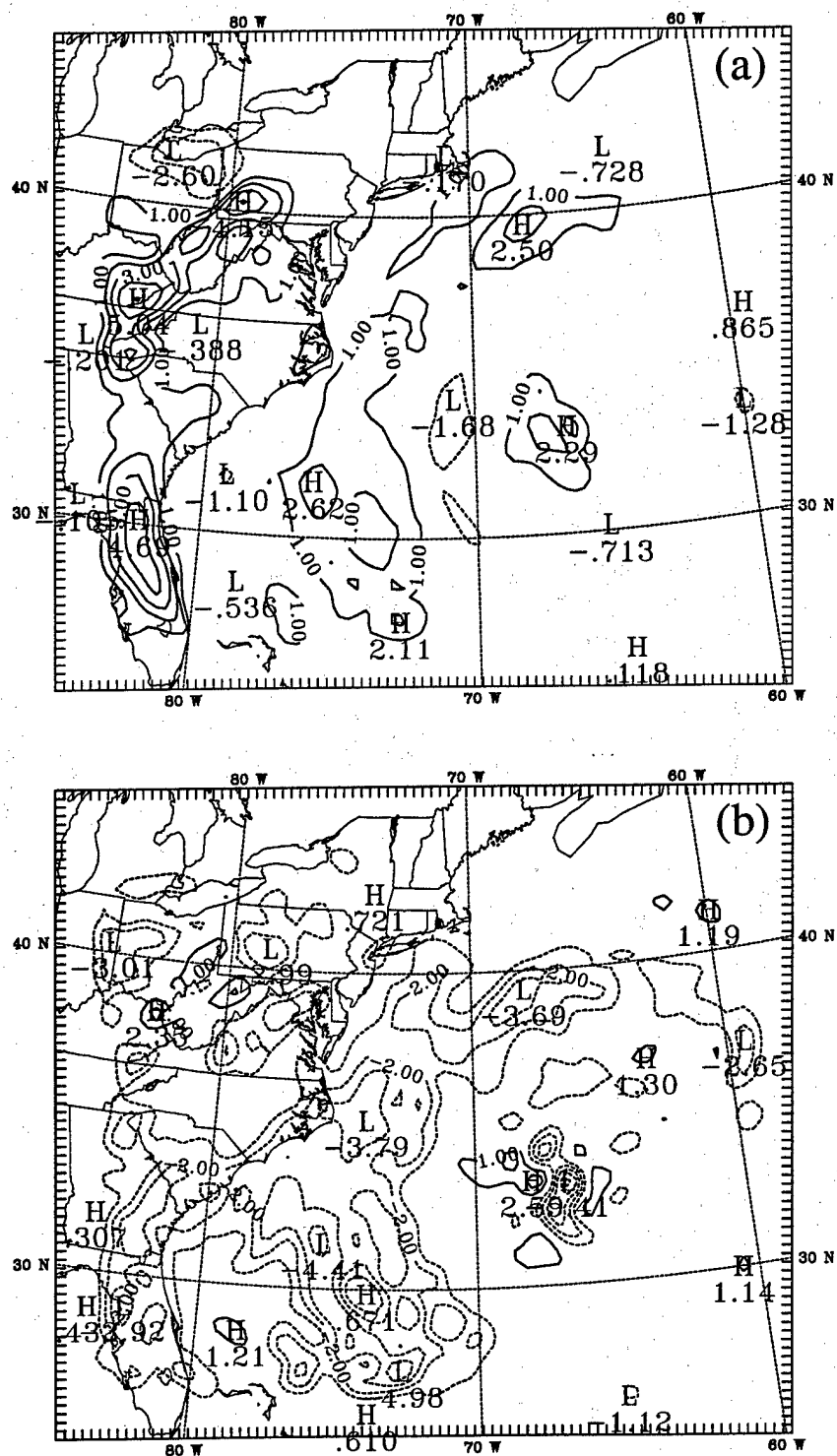
Fig. 9
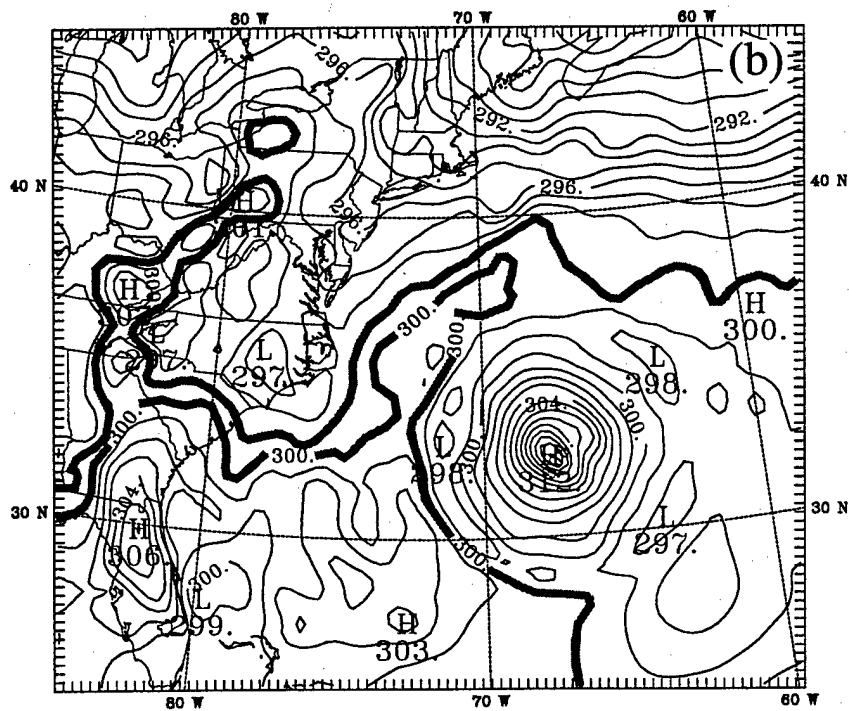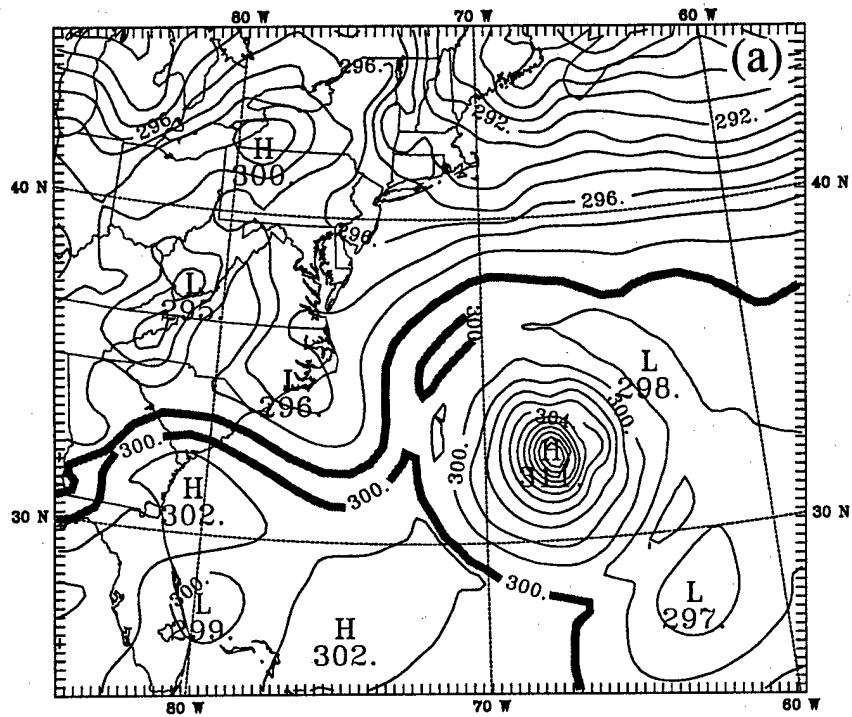
Fig. 10

Fig. 11

Fig. 12

Fig. 13

Fig. 14

CONTOUR FROM -2.0000 TO 22.000 CONTOUR INTERVAL OF 2.0000 PT(3,3)= -2.0211

CONTOUR FROM -4.0000 TO 18.000 CONTOUR INTERVAL OF 2.0000 PT(3,3)= -2.6420

Fig. 15

Fig.16

Fig. 17

1800 UTC 16 AUGUST   BGSAT   1800 UTC 16 AUGUST   BG

1200 UTC 17 AUGUST   BGSAT   1200 UTC 17 AUGUST   BG

Fig. 18

Fig. 19

Fig. 20

1800 UTC 16 AUGUST   BG

(a)

1800 UTC 16 AUGUST   BGSAT

(b)

0600 UTC 17 AUGUST   BG

(c)

0600 UTC 17 AUGUST   BGSAT

(d)

Fig. 21